10-1-2012

DPY-30 Domain and its Flanking Sequence Mediate the Assembly Modulation of Flagellar Radial Spoke Complexes

Radhika Gopal
Marquette University

Kenneth W. Foster
Syracuse University

Pinfen Yang
Marquette University, pinfen.yang@marquette.edu

Published version. *Molecular and Cellular Biology*, Vol. 32, No. 19 (October, 2012): 4012-4024. DOI.

MCB
Journals.ASM.org

The DPY-30 Domain and Its Flanking Sequence Mediate the Assembly and Modulation of Flagellar Radial Spoke Complexes

Radhika Gopal,[a] Kenneth W. Foster,[b] and Pinfen Yang[a]*

Department of Biological Sciences, Marquette University, Milwaukee, Wisconsin, USA,[a] and Physics Department, Syracuse University, Syracuse, New York, USA[b]

RIIa is known as the dimerization and docking (D/D) domain of the cyclic AMP (cAMP)-dependent protein kinase. However, numerous molecules, including radial spoke protein 2 (RSP2) in *Chlamydomonas* flagella, also contain an RIIa or a similar DPY-30 domain. To elucidate new roles of D/D domain-containing proteins, we investigated a panel of RSP2 mutants. An RSP2 mutant had paralyzed flagella defective in RSP2 and multiple subunits near the spokehead. New transgenic strains lacking only the DPY-30 domain in RSP2 were also paralyzed. In contrast, motility was restored in strains that lacked only RSP2's calmodulin-binding C-terminal region. These cells swam normally in dim light but could not maintain typical swimming trajectories under bright illumination. In both deletion transgenic strains, the subunits near the spokehead were restored, but their firm attachment to the spokestalk required the DPY-30 domain. We postulate that the DPY-30–helix dimer is a conserved two-prong linker, required for normal motility, organizing duplicated subunits in the radial spoke stalk and formation of a symmetrical spokehead. Further, the dispensable calmodulin-binding region appears to fine-tune the spokehead for regulation of "steering" motility in the green algae. Thus, in general, D/D domains may function to localize molecular modules for both the assembly and modulation of macromolecular complexes.

The cyclic AMP (cAMP)-dependent protein kinase A (PKA) is a critical regulator in eukaryotic cells. The dimerization and docking (D/D) domain, RIIa, in its regulatory subunit localizes the tetrameric holoenzyme to A-kinase-anchoring proteins (AKAPs). When cAMP binds to the regulatory subunit, the bound catalytic subunits with broad substrate specificity are released to phosphorylate only nearby intended targets. It is well established that the localization via RIIa and AKAP enhances the precision of PKA-mediated regulation spatially and temporally (4, 30). However, the RIIa domain is not unique to PKA. In fact, it is present in more than 200 eukaryotic proteins that lack the other features characteristic of PKA (8, 21, 40, 67, 69). Furthermore, a domain with a similar structural fold, DPY-30 (60), is found in equally numerous proteins. Together, the molecules that share the D/D domain but differ significantly in additional sequences are categorized in the RIIa clan in the Pfam protein family library (http://pfam.janelia.org/). Accumulated evidence suggests that they play important roles unrelated to PKA. For example, DPY-30, a 100-amino-acid (aa) protein existing in various eukaryotes, is a subunit in molecular complexes involved in X chromosome dosage compensation, histone methylation, *trans*-Golgi trafficking, and carcinogenesis (10, 26, 28, 34, 39, 65). Although its only recognizable feature is the DPY-30 domain, in *Caenorhabditis elegans*, defect in it results in lethality of most XX hermaphrodites and a dumpy-shape body of live XO male worms (26). In mammals, DPY-30 is crucial for histone H3K4 trimethylation and cell fate specification of embryonic stem cells (28). Genome-wide transcriptional analysis also implicates the molecule in the assembly or functioning of cilia (57). However, the roles of DPY-30 and the vast majority of RIIa clan members remain largely unknown.

This question can be elucidated by studying its four members in the radial spoke (RS) complex in the flagella of *Chlamydomonas reinhardtii* (Fig. 1). The RS, comprised of at least 19 distinct proteins (69), appears as a "T" or "Y" in electron micrographs (3, 15, 46, 62). The thinner stalk adheres to the 9 microtubule outer doublets of the axoneme, while the bulbous head intermittently contacts the central-pair (CP) apparatus (62). Defects in the RS result in a spectrum of motility deficiencies ranging from jerky flagella to reversible or full paralysis (63, 66, 67, 69). It has been proposed that the periodic engagement between the RS and the CP enables sequential activation of dynein motors on the outer doublets that power rhythmic beating (62, 66). The RS is also implicated in calcium- and phosphorylation-induced changes in flagellar movements (6, 48, 55).

In this report, we focus on DPY-30 domain-containing radial spoke protein 2 (RSP2), which is critical for bridging the bulbous spokehead and the thinner stalk. The *Chlamydomonas* strain pf24 has a start codon mutation in the RSP2 gene (66). The mutation results in paralyzed flagella in which three stalk proteins are diminished, including RSP2 and the other DPY-30 domain-containing protein, RSP23. The spokehead proteins are reduced in abundance, but to a lesser extent (27, 44, 66). The rest of the stalk proteins, including two RIIa domain-containing RSPs, are present in normal amounts. The phenotypes (69), further corroborated by recent cryoelectron tomography of pf24 and the other RS mutants (46) and chemical cross-linking (32), suggest that the two DPY-30 domain-containing RSPs are located in the neck region adjacent to the spokehead, whereas the two RIIa domain-containing proteins are positioned toward the radial spoke stalk base (Fig. 1D and Table 1). However, pf24 phenotypes are not conducive to

Received 22 November 2011 Returned for modification 20 December 2011
Accepted 19 July 2012
Published ahead of print 30 July 2012
Address correspondence to Pinfen Yang, pinfen.yang@marquette.edu.
* Present address: Radhika Gopal, Department of Molecular Biology, Scripps Research Institute, La Jolla, California, USA.
Supplemental material for this article may be found at http://mcb.asm.org/.

doi:10.1128/MCB.06602-11

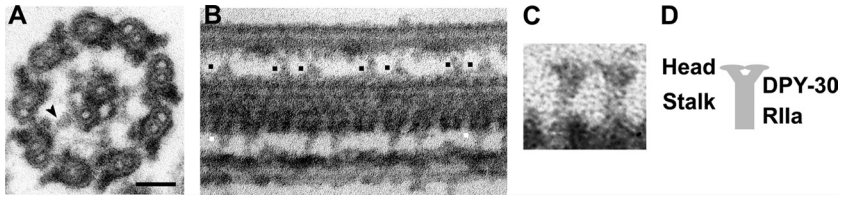

FIG 1 Morphology of the radial spoke complex that harbors RIIa and DPY-30 domain-containing subunits. (A) Electron micrograph of a cross-sectioned axoneme in a *Chlamydomonas* flagellum. The T-shaped RS is indicated by an arrowhead. Scale bar, 50 nm. (B) RSs appear as doublets (black dots) in each 96-nm repeat in the longitudinal section. In some RSs, the center of the enlarged spokehead appears hollow (white dots). (C) The section in which the central pair is dissociated reveals a clear morphology of the spokehead region. (D) Schematic depicting the RS and the predicted locations of the RSPs containing either an RIIa or a DPY-30 domain.

inferring the specific roles of RSP2 and its DPY-30 domain because of the deficiencies in multiple spoke subunits. Intriguingly, although RSP2 is critical for RS assembly, it binds calmodulin, a molecule implicated in regulating the beating of various cilia and flagella (7, 43), presumably through a C-terminal region (70). An adjacent region is predicted to be a degenerate GAF domain known for binding small ligands (1). However, these features, which occupy 80% of the RSP2 sequence, are not evolutionarily conserved. Only the DPY-30 domain and a short flanking helix with coiled-coil propensity are common in potential RSP2 orthologues. We hypothesize that the DPY-30 domain tethers the conserved helix for RS assembly required for oscillatory beating, while the calmodulin-binding extension is involved in a flagellar behavior unique to *Chlamydomonas*. To test this, new RSP2 transgenic mutants were created to avoid severe assembly defects. The phenotypes of these new transgenic strains support the hypothesis and demonstrate that the D/D domain, which is known to localize PKA, also targets functional moieties for the assembly and modulation of molecular complexes.

MATERIALS AND METHODS

Strains, culture conditions, RSP2 gene, and biochemistry. *C. reinhardtii* strains, culture conditions in Tris-acetate-phosphate (TAP) medium, purification of axonemes, sucrose gradient fractionation of RS, RSP2 genomic DNA, and RSP2 expression constructs were described previously (66).

Construct design. The NcoI RSP2 genomic fragment was released from an RSP2 phage clone (70) and ligated into the pGEM-T Easy vector. This plasmid was used as the wild-type (WT) control and as a template to generate a series of mutant constructs. To create the ΔDPY-30 construct, the fragments flanking the DPY-30 coding sequence were amplified using the following primer pairs, named after the restriction sites in the RSP2 gene: (i) Bam (CTTCTACACGGATCCGCCGGTCTCC) and Hind H′ (CGAAGCTTTTGGGTCGGAGCCATTCTTGAGTGTC) and (ii) Hind H″ (AGAAGCTTCTGGGCCTATGGCTGCTCAAGTAAGC) and Nru (C AAATCCTGTTGCCGCTCGCGA).

The PCR product of Bam-Hind H′ (1,000 bp) and Hind H″-Nru (150 bp) replaced the Bam-Nru fragment in the wild-type RSP2 plasmid. To create a 3′-tagged $RSP2_{1\text{-}120}$ (1-120) construct, the p3HA plasmid (54) was first converted into p3HA6His using a PCR approach and primers containing His codons. The tagged sequence was amplified again to add EcoRI and XbaI restriction sites. Meanwhile, the RSP2 gene was PCR amplified using primers Bam and Eco (TGGGAATTCGGCTGTGTGCT GCTTGACCAG). The PCR products of Bam-Eco (1,600 bp) and the 150-bp 3HA6His sequence were cloned between the BamHI site and an XbaI site that was inserted before the stop codon of the wild-type RSP2 vector.

To generate the CaMB* construct, the pET28a-RSP2 expression construct (70) was used as a PCR template. First, QuikChange site-directed mutagenesis (Stratagene) was carried out to alter the 2nd CaMB motif with the primer pair CalB5′ (CATCAAGCAGGTGCGGGAGGTGGCGG ACAAGGCAGT) and CalB3′ (GCAGCACTGCCTTGTCCGCCACCTC CCGCACCTGCT), in which the R581 and R584 codons were replaced with a glycine codon. This construct was used for expressing CaMB* in the bacterial strain BL21(DE3) (70). In addition, the 440-bp region containing the mutated sequence was released by BsrGI and XhoI digestions and cloned into the control genomic plasmid for transformation of *C. reinhardtii* strain pf24. To create the ΔCT-Tag construct, p3HA6His was amplified using the p3HA plasmid (54) as a template and primers HAXhoS (ACTCGAGCAGCCGGGGAGGCCTGTCGCGA) and HAXhoAS (TCT CGAGTCTAGATCAGTGGTGGTGGTGGTGG), which included a stop codon. The 150-bp tag sequence was cloned into a convenient XhoI site preceding the stop codon. This cloning strategy resulted in the addition of a 3HA6His tag and deletion of the C-terminal 16 aa. The ΔCT construct, without any tag, was created by amplifying the wild-type construct with the primer pair BsrG (GACGCGGAGATGCCGAACACGCTG) and Xho (GCTGCTCGAGCTTTAGTTCGACCCCTCCTGGGCCGGCTG), which included a stop codon. The PCR product (440 bp) with a stop codon replaced the original sequence in the wild-type plasmid.

To express the RSP2 N-terminal region, PCR fragments encoding aa 7 to 119 and 7 to 265 were cloned into the pMCSG19 vector behind a maltose binding protein (MBP) coding sequence, a proteolytic site, and a His tag (17) by the Midwest Center for Structural Genomics (http://bioinformatics.anl.gov/mcsg/technologies/structuredetermination.html). The region was chosen based on predicted solubility and crystallization. The MBP-tagged recombinant proteins were used to test calcium-dependent calmodulin binding as

TABLE 1 Phenotypes of RSP2 transformants and paralyzed RS mutants

Parameter	Value in strain: Cont	pf14[a]	pf1 and pf17[a]	pf24[a,b]	ΔDPY	1-120	CaMB*	ΔCT-Tag
Velocity[c] (μm/s)	111 ± 31	Pf	Pf	Pf	Pf	99 ± 27	112 ± 39	Varies
RSP defects	None	All	1, 4, 6, 9, 10	1, 4, 6, 9, 10, 2, 23, 16	None	None	None	Varies

[a] Reference 27. pf14 is spokeless, pf1 and pf17 lack the spokehead, and pf24 is the parental strain from which new RSP2 transgenic mutants were generated.
[b] References 44 and 66.
[c] Pf, paralyzed flagella. The velocity of motile strains was derived from the measurements of 12 randomly selected cells recorded under dim light.

described previously (70). The aa 7 to 119 fragment released by the coexpressed protease was Ni-nitrilotriacetic acid (Ni-NTA) purified for raising the anti-RSP2 antibody.

Transformation. All constructs were cotransformed by electroporation (53) into the RSP2 mutant, pf24, with the pSI103 plasmid, which confers paromomycin resistance. Briefly, autolysin-treated cells were washed with TAP medium containing 40 mM sucrose and resuspended in the same solution to a final concentration of 1×10^8 cells/ml. A 125-μl aliquot was placed in a 2-mm electroporation cuvette (model 620; BTX Technologies, Inc.) and subjected to an electric pulse (ECM 630 electroporation apparatus; BTX Technologies, Inc.) of 360 V for 2 milliseconds (equivalent to 500 V/capacitance and resistance, 25 μF capacitance and 125 Ω). The cells were allowed to recover for 60 min under light after addition of 10 ml TAP-sucrose solution. After 1 h, the cells were centrifuged gently and washed three times with TAP buffer. Finally, the cells were resuspended in TAP buffer and allowed to recover overnight. After 24 h, the cell suspensions were plated on TAP agar plates with 10 μg/ml paromomycin.

Single colonies that formed after 4 to 5 days were transferred to fresh TAP plates and subsequently resuspended in TAP medium in 96-well plates for initial motility analysis using an inverted or upright compound microscope (Olympus IX51 and BH-2). For each construct, approximately 200 antibiotic-resistant clones were resuspended in water or TAP medium and screened microscopically. Only the flagellar behaviors that were exhibited by more than 10 clones from at least two different transformation reactions were considered possible phenotypes for the exogenous RSP2 polypeptides. The cells were cultured in liquid medium for axoneme preparation. Western analysis of axonemes probed with anti-RSP2 antibody or antihemagglutinin (anti-HA) antibody confirmed the presence of RSP2 polypeptides, equally abundant in the fully swimming strains but varying in abundance in the completely or partially paralyzed strains. Only the strains in which RSP2 polypeptides were optimally restored in the flagella were further analyzed.

Motility analyses. The motility analyses were performed as described previously (66, 67). For low-speed video microscopy, cells were digitally recorded under ×200 bright-field light microscopy using a charge-coupled device (CCD) camera (CoolSNAP ES; Photometrics) at a maximum rate of 20 frames per second and a Plan Fluor 20× objective (0.50 numerical aperture [NA]; Nikon). The MetaMorph imaging system (version 6.1r5; Molecular Devices, Sunnyvale, CA) was used for tracking the movement of individual cells and determining swimming velocities. For high-speed video microscopy, a MotionPro HP-3 camera (Redlake) was used to record at a rate of 500 frames per second with a Plan Apo 40× objective and a 400× bright-field light compound microscope (Nikon). A gooseneck lamp with two fiber optic guides and a tungsten light source (model DL-150; Fryer Company, IL) replaced the illumination from the microscope for altering the illumination direction.

For testing calcium dependence, cells were resuspended in 10 mM HEPES, with or without 0.4 mM EGTA or 1 mM calcium, or in growth medium as a control. The cells were observed immediately and every 5 min under dim and normal light settings. The light intensity was measured using a light meter (model 840010; Sper Scientific, AZ).

Sequence analysis. Molecular modules were identified using the SMART (http://smart.embl-heidelberg.de/) and COILS (http://www.ch.embnet.org/software/COILS_form.html) programs. Sequence alignments were generated with the ClustalW2 program (http://www.ebi.ac.uk/Tools/clustalw2/index.html). BLASTP searches were conducted using the default parameters. Homology modeling and molecular presentation were generated using the SWISS-MODEL 8.5 server (http://swissmodel.expasy.org//SWISS-MODEL.html) and the PyMOL program (http://www.pymol.org).

RESULTS

Sequence analyses of the RIIa and DPY-30 domains in the radial spoke proteins. It has been demonstrated that both RSP7 and RSP11 have an RIIa domain, while RSP2 has a DPY-30 domain (69). A subsequent motif search revealed a DPY-30 domain in RSP23 and its orthologue, NDK-5. These four spoke proteins are listed as members of the RIIa clan in the Pfam database. As shown by sequence analysis, these ~40-aa domains are predicted to fold into a helix-loop-helix structure with proline and hydrophobic residues located at similar positions (Fig. 2A, shaded in black and gray). Homology modeling of the domains from RSP11 and RSP2 against the crystallographic algorithms of the respective domains from mammalian RII and DPY-30 (23, 60) demonstrated similar homodimeric structures, except for a short region preceding helix I: a beta strand in the RIIa domain and a helix I′ in the DPY-30 domain (Fig. 2B). Different N termini could affect the molecular interactions of the D/D domains (20) and are consistent with the distinct locations of the RIIa and DPY-30 domain-containing RSPs in the RS (Fig. 1D) (69).

Although the importance of RSP2 in RS assembly and flagellar beating suggests that RSP2-like molecules might be present in most motile cilia and flagella, a BLASTP search showed that only a few protists and moss have RSP2-like molecules that share similarity with the entire 738-aa sequence, especially the first 120 aa. However, a BLASTP search using only the N-terminal region as a query revealed numerous hits, including DYDC2 (DPY-30 domain-containing protein 2) (Fig. 3), the vertebrate protein that most resembles RSP2. The human DYDC2 gene (Gene ID 84332) is adjacent to a highly homologous gene encoding DYDC1, possibly arising from a gene duplication event. We discuss only DYDC2 because of the similarity. As expected for an RSP2 orthologue, DYDC2 was found in the human cilium proteome and is listed in the cilium proteome database (2, 42). Inferred from expressed sequence tags (EST), it is enriched in the lung and the testis, which contain cells with motile cilia or flagella (Hs.512782 in the UniGene database [http://www.ncbi.nlm.nih.gov/]). However, it has only ~200 aa, lacking the degenerate GAF domain (1) and the calmodulin-binding motifs (70). The similarity between RSP2 and DYDC2 is primarily limited to the N-terminal 120 aa, with 45% identical residues in the DPY-30 domain (Fig. 3A, underlined) and 18% in the flanking region. Notably, despite the limited similarity of the flanking sequence, the COILS program predicts that this region in both molecules will form an α-helix with coiled-coil propensity (Fig. 3B), which is known for mediating protein-protein interactions. Similarly, the putative vertebrate orthologue of the DPY-30 domain-containing RSP23, NDK-5 (44), also lacks RSP23's extended C-terminal region with three calmodulin-binding IQ motifs (Fig. 3C). One possibility is that DYDC2 and NDK-5 are the orthologues of RSP2 and RSP23, respectively, and the additional sequences in the two *Chlamydomonas* DPY-30 domain-containing molecules are dispensable for flagellar beating. Based on these observations, we postulate that the conserved DPY-30 domain and the coiled-coil-forming helix in RSP2 are involved in RS assembly and that the additional C-terminal region mediates a dispensable calmodulin-dependent reaction.

The conserved DPY-30 domain and adjacent helix in RSP2 are sufficient for RS assembly and oscillatory beating. If the hypothesis is correct, *Chlamydomonas* cells expressing only the conserved first 120 aa in RSP2 will have motile flagella with all RSPs critical for flagellar beating but cannot display the calmodulin-dependent behavior. Conversely, cells defective in the conserved region will not assemble functional RSs, and consequently, their flagella will be paralyzed. As it is not feasible to generate *Chlamy-*

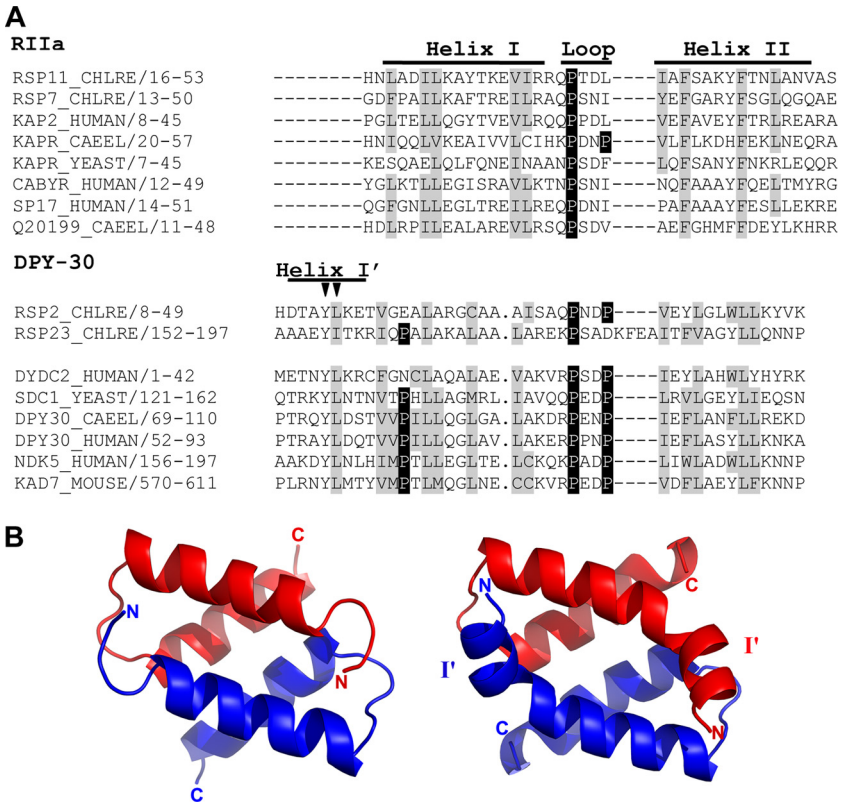

FIG 2 Four *Chlamydomonas* radial spoke proteins contain a typical RIIa or DPY-30 domain. (A) Sequence alignment of the RIIa and DPY-30 domains in the four RSPs and representative molecules from human, *Saccharomyces cerevisiae*, and *C. elegans*. The D/D domain is comprised of a helix-loop-helix structure (marked with lines above the alignment) with conserved hydrophobic residues and prolines (shaded gray and black, respectively). The key difference between the two domains is in the N terminus: only helix I in the DPY-30 domains is preceded by helix I′ with two conserved residues (arrowheads). (B) The tertiary conformation of RIIa (left) and DPY-30 (right) domains. The additional helix I′ (I′) forms the lateral boundary of the docking pocket defined by helix I. The sequences from RSP11 (aa 14 to 51) and RSP2 (aa 9 to 50) are modeled, respectively, after the crystallographic algorithms of the mouse RIIa domain (Protein Data Bank [PDB] ID, 2IZY) (23) and the human DPY-30 domain (PDB ID, 3G36) (60).

domonas mutants by homologous recombination, we used a well-established strategy (14), expressing RSP2 polypeptides, full length or mutated (Fig. 4A), in the paralyzed RSP2 mutant, pf24, that produces a trace amount of full-length RSP2 (27).

The wild-type RSP2 gene (70) was cloned and used as a PCR template to create three truncation constructs (Fig. 4B) that lack the DPY-30 domain (ΔDPY), the extended C terminus ($RSP2_{1\text{-}120}$), or the C-terminal 16 aa (ΔCT-Tag). To aid in detection of truncated

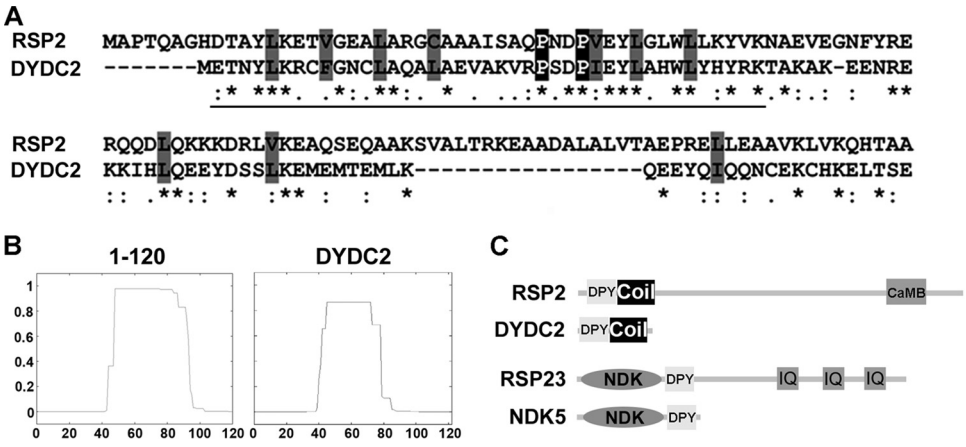

FIG 3 Conserved features in RSP2 and its human homologue DYDC2. (A) Sequence alignment of the N-terminal 120 amino acid residues. The similarity is particularly prominent in the DPY-30 domain (underlined). Asterisk, identity; colon, high similarity; dot, low similarity; gray shading, conserved hydrophobic residue. (B) Coiled-coil propensity in the less conserved region downstream of the DPY-30 domain. The graphs were generated by the COILS program using a window width of 28. (C) Schematic showing that the extended C termini in the two DPY-30 domain-containing radial spoke proteins are absent in their human homologues.

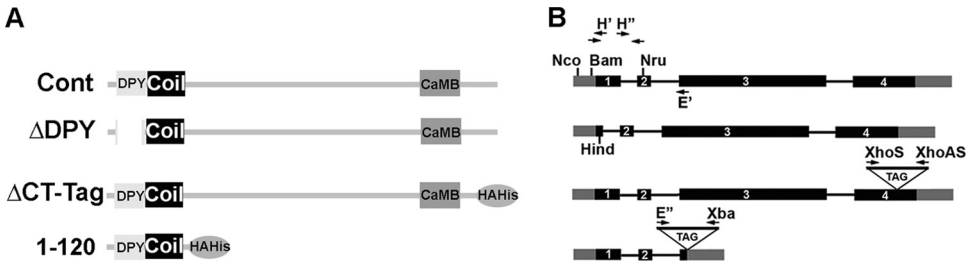

FIG 4 Mutagenesis of the RSP2 gene. (A) RSP2 deletion polypeptides. Cont is the wild-type RSP2. ΔDPY lacks 32 aa in the DPY-30 domain. ΔCT-Tag RSP2 lacks the C-terminal 16 aa but contains a tag with 3 HA and 6 His epitopes (HAHis). $RSP2_{1-120}$ contains the conserved DPY-30 domain, the downstream coil-forming helix, and the HAHis tag. (B) PCR strategies for creating genomic deletion constructs. Primers are indicated by arrows. The ΔDPY construct was generated using 2 primer pairs: Bam and Hind-H′ (H′), and Hind-H″ (H″) and Nru. Ligation of the two PCR products resulted in deletion of the DPY-30 domain. The two C-terminal-truncation constructs were generated similarly using primer pairs Bam-E′, E″-Xba, and XhoS-XhoAS. The last two primer pairs amplified the sequence for the HAHis tag and a stop codon.

polypeptides, a tag that encodes 3 HA epitopes and 6 His residues was inserted into several truncated constructs, as indicated. Each of these constructs was transformed into pf24, along with an antibiotic selection plasmid. For each group, ~200 antibiotic-resistant clones were screened by light microscopy. The results are summarized in Table 1.

As expected, all clones from the transformation with only the antibiotic-selection plasmid were paralyzed, like pf24. In the wild-type control group, 12 clones (5.2%) behaved like wild-type cells—all flagellated cells were motile and were used as controls (Cont). All clones in the ΔDPY-30 group were paralyzed. However, compared to pf24 flagella, which rarely crossed each other (Fig. 5, top), 11 ΔDPY-30 clones (10.4%) had flagella that crossed each other sporadically (Fig. 5, bottom), a phenotype also exhibited by the mutants defective in the spoke HSP40 (66) or the kinesin (72) in the CP. For the $RSP2_{1-120}$ group, 10 clones (4%) were fully motile but exhibited a novel light-induced behavior that was absent in the control (see below). Taken together, these results indicate that the first 120-aa region is sufficient for rhythmic beating and that the DPY-30 domain in this region is critical. Unexpectedly, ΔCT-Tag or the untagged ΔCT polypeptide (not shown), albeit lacking only the last 16 amino acid residues, is less effective in rescuing pf24 than $RSP2_{1-120}$. Ten ΔCT-Tag clones (3%) contained swimmers, as well as paralyzed cells. None of the clones had 100% swimmers.

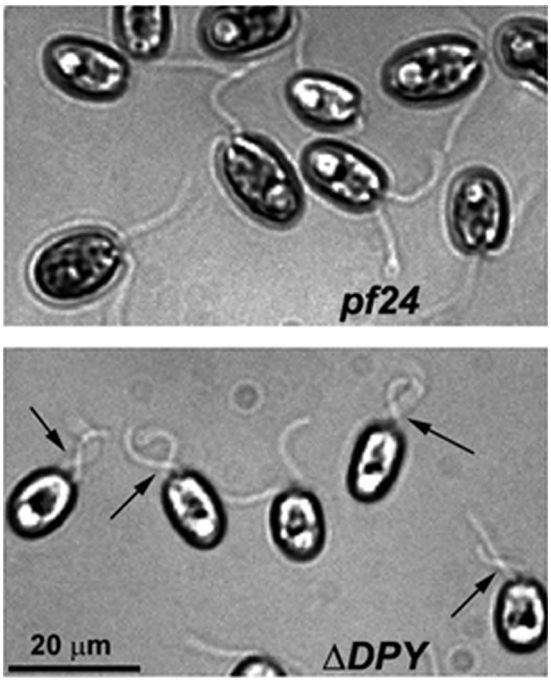

FIG 5 The DPY-30 domain in RSP2 is required for oscillatory beating. The parental pf24 cells (top) and the cells transformed with the ΔDPY construct (bottom) are paralyzed, but their paralyzed flagella appear distinctly. While the flagella of most pf24 cells stretch out in a V (top), the two flagella of many cells in a few ΔDPY clones jerk intermittently, crossing each other often (bottom, arrows). The images were taken from live cells using a CCD camera at a rate of ~20 frames/s.

Western blots of axonemes from representative clones in each group (Fig. 6A) confirmed that the expected mutated RSP2 polypeptides were restored. To assess RS assembly, we used Western blots to reveal the relevant RSPs in axonemes from the representative deletion transgenic strains. RSP3, which was normal in pf24, served as a loading control. Both ΔDPY (Fig. 6B, left, arrowhead) and $RSP2_{1-120}$ (right, arrowhead) were restored to the axonemes. ΔDPY migrated slightly faster than the diminished full-length RSP2 (dots) from pf24 and was as abundant as the control. The other RSPs, which were absent in the spokeless pf14 and deficient in pf24 (first two lanes), including spokehead proteins (represented by RSP1) and the predicted neck proteins (RSP23 and RSP16), appeared fully restored in the motile $RSP2_{1-120}$ strain, as expected, and, surprisingly, were fully restored in the paralyzed ΔDPY strain, as well (last four lanes). This indicates that the DPY-30 domain, although crucial for flagellar beating (Fig. 5), is dispensable for restoring the RS composition, and thus, the DPY-30 domain flanking region that is present in both ΔDPY and the $RSP2_{1-120}$ strain and has coiled-coil propensity is involved in the assembly role of RSP2. RSP23 migrated as multiple bands, and the band patterns in different axonemes varied, like those in the other spoke mutants and dynein mutants (44, 66). The cause of the variations remains unclear but does not seem to be related to the motility level because RSP23 band patterns in motile (1-120) strains and paralyzed (ΔDPY) strains are similar (Fig. 6C). The variations could be due to RSP23's susceptibility to proteolysis (44) or stochastic autophosphorylation by its NDK activity (33). Calmodulin was not probed because a change in the calmodulin content in axonemes with defective RSs is not expected to be evident against a background of this molecule from other axonemal complexes (16, 18, 43, 61).

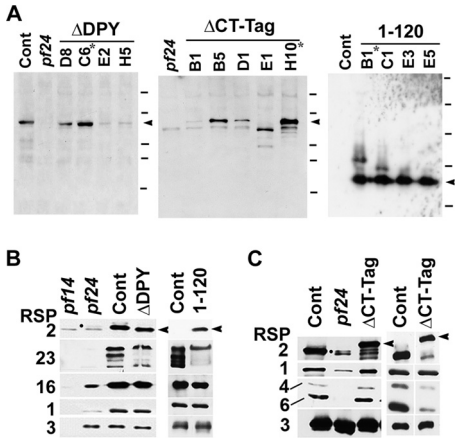

FIG 6 Truncated RSP2 polypeptides restored RS composition. (A) Representative Western blots for screening transgenic strains. Axonemes were harvested from pf24 and from the transformants that exhibited phenotypes distinct from that of pf24. ΔDPY and ΔCT-Tag were revealed by anti-RSP2 antibody. The sizes of the protein markers are 170, 130, 100, 70, and 55 kDa. $RSP2_{1-120}$ was revealed by anti-HA antibody. The sizes of the protein markers are 55, 40, 35, 25, and 15 kDa. All three deletion RSP2 polypeptides (arrowheads) migrated differently from the full-length RSP2 in the control (Cont). The amounts of $RSP2_{1-120}$ from all four strains that contained nearly 100% swimmers were similar, whereas the RSP2 polypeptides from ΔDPY and ΔCT-Tag strains that contain paralyzed cells varied in abundance. The shorter-than-expected RSP2 from strain E1 is likely due to truncation of the inserted transgene. The strains with the most abundant RSP2 polypeptides (asterisks) were further analyzed in panels B and C. (B) Western blots of similar amounts of axonemes from representative transgenic strains expressing ΔDPY or $RSP2_{1-120}$ (arrowheads) or full-length RSP2 (Cont). The blots were probed for relevant RSPs as indicated, including RSP1 in the spokehead and RSP2, RSP16, and the phosphoprotein RSP23 in the nearby neck region. These spoke proteins, which were largely absent in the spokeless pf14 and deficient in pf24, were equally abundant in the ΔDPY, $RSP2_{1-120}$, and Cont strains. Note that the trace amount of endogenous RSP2 (dot) in pf24 *co*migrated with the full-length RSP2 in Cont and was distinct from an adjacent background band that was also present in the negative-control pf14. RSP3 served as a loading control. (C) The RS composition in ΔCT-Tag axonemes was affected by culture conditions. All RSPs tested, including the ΔCT-Tag polypeptide (arrowhead), appeared equally abundant in axonemes prepared from log-phase cultures (left). However, the abundances of RSP4 and RSP6 paralogues (lines) in the spokehead were obviously reduced if axonemes were prepared from stationary-phase cultures in which most ΔCT-Tag cells were paralyzed (right). In contrast, the assembly of these two paralogues in Cont was evidently not affected by culture conditions. ΔDPY and ΔCT-Tag were revealed by anti-RSP2 antibody. The $RSP2_{1-120}$ blot was probed with anti-HA, and thus, wild-type RSP2 in Cont was not revealed.

The mixed population of motile and nonmotile cells in ΔCT-Tag cultures is also a phenotype of pf26 allelic mutants that are defective in the gene encoding one of the two spokehead paralogues, RSP6 (13, 63). The motile fraction in pf26 cultures decreases when the medium becomes exhausted, and the reduction was correlated with decreased spokehead assembly in axonemes (63). To test if RS assembly in ΔCT-Tag strains was as medium sensitive as in pf26, their axonemes were harvested at two different time points (Fig. 6C). The RSPs from log-phase cultures that contained both motile and nonmotile cells appeared similar to that of the control, including the two spokehead paralogues, RSP4 and RSP6 (Fig. 6C, left, lines). However, they were evidently diminished in the ΔCT-Tag samples from stationary-phase cultures, which contained largely nonmotile cells (right), despite normal abundance of ΔCT-Tag RSP2 and the third spokehead protein, RSP1. This indicates that the fraction of paralyzed cells in ΔCT-Tag strains is not caused by transgene silencing but instead is due to medium-sensitive assembly deficiency. These results suggest that RSP2 projects its C-terminal tail toward the spokehead, and without the last 16 aa in RSP2, spokehead assembly is compromised, possibly due to misfolded RSP2 polypeptides.

The defective RSP2 gene in pf24 expressed a trace amount of full-length RSP2 (Fig. 6C, dot). Although this fraction may lessen the severity of the phenotypes from RSP2 deletion polypeptides expressed in pf24, its effect appears minor because of drastic differences in the flagellar phenotypes of the parental pf24 and new transgenic strains with abundant mutated RSP2 polypeptides in flagella.

The DPY-30 domain is critical for anchoring the flanking sequences to the spokestalk. The motility phenotypes suggested that although truncated RSP2 polypeptides could restore RS composition, the assembly was abnormal. To test this, RSs were extracted from axonemes and subjected to velocity sedimentation on sucrose gradients. Western blots of gradient fractions showed that all RSPs from the wild-type control sedimented in a single 20S peak as intact particles (Fig. 7A, top). However, in the gradients of the transgenic mutants lacking the DPY-30 domain (middle) or the C terminus (bottom), the components around the spokehead region were dissociated. Spokehead proteins and the neck proteins, including ΔDPY and RSP16 (HSP40), sedimented as small particles distinct from the remaining stalk (represented by RSP3). Thus, although these RSPs are restored to the RS by ΔDPY-30 and $RSP2_{1-120}$ polypeptides, they are unstable. In contrast, RSP23, $RSP2_{1-120}$, and RSP2 (Fig. 7A, open arrows), all containing a DPY-30 domain, cosedimented with the major stalk protein, RSP3, suggesting that the DPY-30 domain secures the association of RSP2 and RSP23 with the remaining stalk.

RSP2 binds calmodulin in a calcium-dependent manner and contains three potential calmodulin-binding sites, two at aa 540 to 592 (70) and one at aa 190 to 208 (71; http://calcium.uhnres.utoronto.ca/ctdb/pub_pages/general/index.htm). To test this, sucrose gradient fractions were probed for calmodulin. As shown previously (68), calmodulin sedimented into three peaks in the control gradient (Fig. 7B, top). The first 20S calmodulin peak was absent in the $RSP2_{1-120}$ gradient (Fig. 7B, compare top and middle), consistent with the absence of the 20S RS peak in the gradient (Fig. 7A, bottom). However, it was unclear if the smaller RS particles in the $RSP2_{1-120}$ gradient contained less calmodulin because of the proximity of the other calmodulin-containing complexes in the adjacent fractions (16, 18, 61). Second, we tested calmodulin binding on four bacterially expressed RSP2 polypeptides: the WT, CaMB*, aa 7 to 119, and aa 7 to 265. For CaMB*, two arginine residues in the last positively charged calmodulin-binding motif were replaced with glycine (R581G and R584G). The two truncated polypeptides were expressed as fusion proteins with an N-terminal MBP tag that is compatible with calmodulin affinity purification (64) and improves the solubility and expression level (17). Like RSP2 (70), CaMB*, with only one site mutated, still exhibited calmodulin affinity, as demonstrated by their reduction after incubation with calmodulin-conjugated agarose (Fig. 7B, bottom, compare lanes Pre and Post) and their elution by 2 mM EGTA. In contrast, the two truncated polypeptides did not show significant binding, suggesting that the calmodulin-binding region is in the C terminus, downstream of the first 265 amino acid residues.

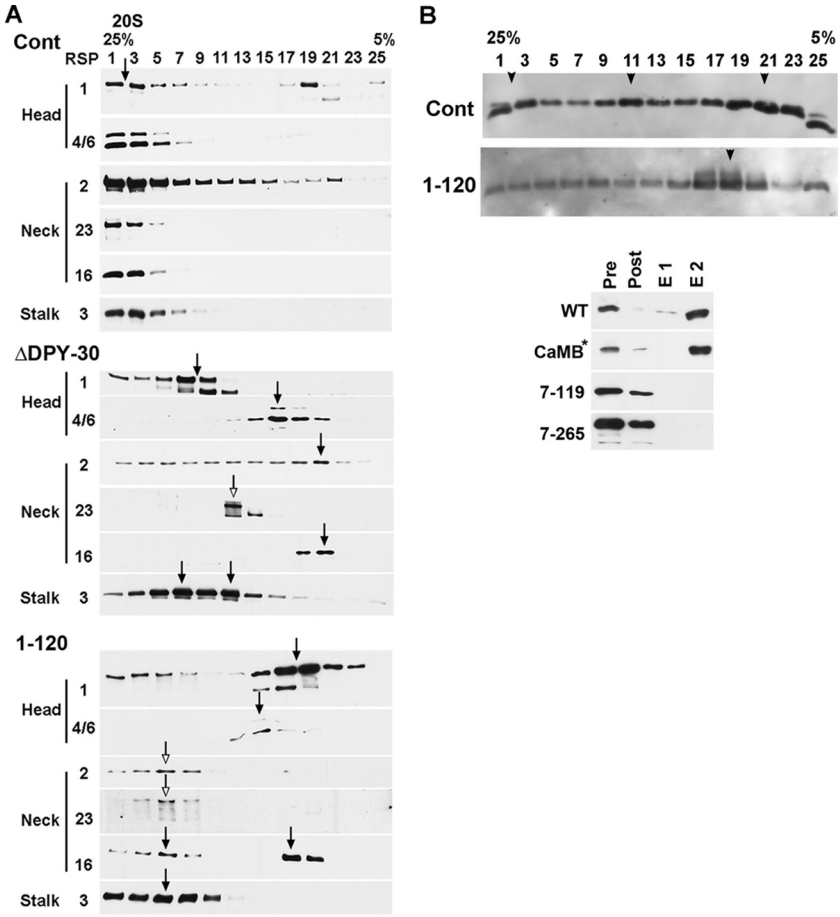

FIG 7 Altered molecular interactions in the RS complex with mutated RSP2. (A) Instability of the spoke proteins near the head-stalk juncture of the RS with partial RSP2 polypeptides, with the exception of the polypeptides containing a DPY-30 domain. Sucrose gradient fractions of the axonemal extract were analyzed with Western blots probed for proteins as indicated. In the gradient of the wild-type control (top), all RSPs, including RSP1, -4, and -6 in the spokehead; RSP2, -16, and -23 in the neck region; and the stalk, represented by RSP3, sedimented together as a single 20S peak (solid arrows). These components in the gradients of ΔDPY (middle) and $RSP2_{1-120}$ (bottom) axonemal extracts no longer cosedimented with RSP3, except DPY-30 domain-containing RSP2 polypeptides and RSP23 (open arrows). (B) Deletion of RSP2's C-terminal tail perturbed the interaction of RSP2 and calmodulin. Calmodulin sedimented as three peaks in the control gradient. The first peak, corresponding to the 20S RS, was absent in the $RSP2_{1-120}$ gradient (top), which lacks the 20S RS peak (A, bottom). In the presence of 2 mM calcium, calmodulin-agarose affinity purification pulled down recombinant full-length RSP2 polypeptide or CaMB*, a full-length RSP2 in which two positively charged arginine residues in the last predicted calmodulin-binding site were replaced with glycine residues (R581G and R584G). However, calmodulin affinity is not evident for RSP2 fragments with aa 7 to 119 and 7 to 265. The N termini of these two RSP2 fragments were tagged with MBP for improved expression and solubility. Pre, bacterial supernatant; Post, flowthrough; E1 and E2, two consecutive eluents with 2 mM EGTA. All polypeptides were revealed by Western blots probed for molecules, as indicated.

The intensity and orientation of illumination affect the trajectories of $RSP2_{1-120}$ cells. Although $RSP2_{1-120}$ cells were motile, they appeared more agitated than the control at the initial screening when viewed with either an upright or an inverted microscope. Their movement appeared irregular and brisk. However, the difference was not as evident when the light intensity was reduced or a red filter blocked much of the short-wavelength light to which *Chlamydomonas* is sensitive (25, 38, 41), indicating that this behavior was light dependent. Video microscopy (see Videos 1 to 3 in the supplemental material) and tracking of individual cells from three representative strains showed that the trajectories of $RSP2_{1-120}$ cells were similar to those of the control in dim light (D) (60 lx) (Fig. 8A, compare the left images of the control [Cont] and 1-120) but became much more irregular when the light intensity was increased to the normal level routinely used for microscopy (N) (1 klx) (middle column). The trajectories quickly returned to linear/helical when the light intensity was decreased again (right column). Thus, the irregular movement was triggered by brighter light and was reversible. Similar behavior was also observed in three CaMB* strains (Fig. 8A, bottom row) in which the last predicted calmodulin-binding motif in the genomic construct was mutated. Consistent with the effect of light, which causes an increase in the intracellular calcium concentration (25), the irregular trajectories were not as evident when the free-calcium concentrations in the solution were reduced (Table 2). This suggests that the C-terminal calmodulin-binding region in RSP2 is involved in a calcium-dependent steering behavior. The velocity of $RSP2_{1-120}$ cells recorded under dim light appeared only slightly lower than those of the other two strains (Table 1).

It has been demonstrated that calcium changes the beat frequency, waveform, phototaxis, and photoshock by affecting dynein motors (31, 37, 56), as well as nondynein complexes, such as

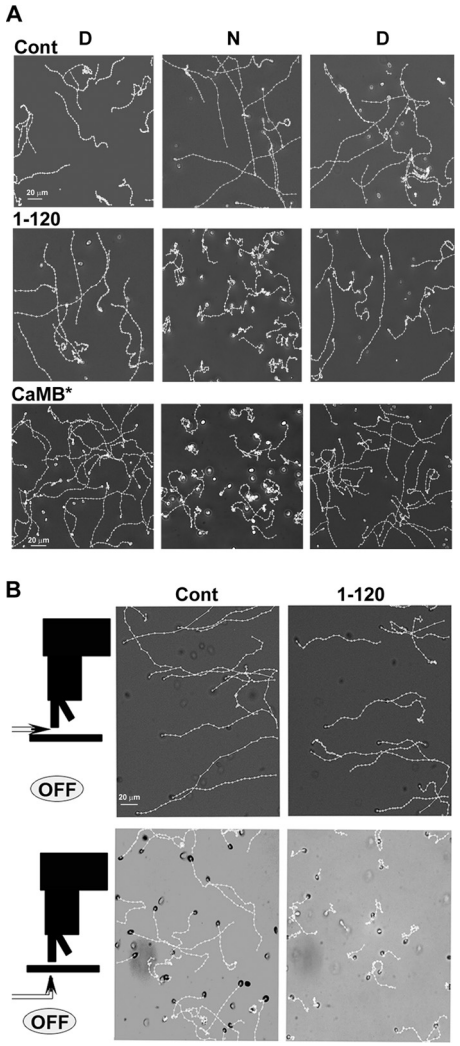

FIG 8 Light intensity and orientation affect the movement of $RSP2_{1-120}$ cells. (A) Light microscopy imaging and tracking of cells in log-phase cultures. The trajectories of wild-type control cells (Cont, top row) were largely helical when the light intensity was shifted between dim (D) (60 lx) and normal (N) (1 klx). In contrast, the trajectories of $RSP2_{1-120}$ cells were helical in dim light but irregular in normal light intensity (1-120, middle row). The cells that expressed full-length RSP2 in which two residues in a CaMB motif were mutated (CaMB*, bottom row) also exhibited light-induced irregular trajectories. (B) The irregular trajectory was induced by the bright light perpendicular to the glass surface. Control and $RSP2_{1-120}$ cells swam in mostly helical paths when light (6 klx), provided by the fiber optic of a gooseneck tungsten lamp, was parallel to the glass slide (top, arrow). The trajectories of $RSP2_{1-120}$ cells became particularly irregular when the fiber optic was placed perpendicular to the slide. The light from the microscope was turned off (OFF).

the RS (6, 52). However, these features in $RSP2_{1-120}$ strains appeared normal. In a typical photoaccumulation assay for testing phototaxis (41) using a dual fiber optic-guided gooseneck tungsten lamp with a direction parallel to the bottom of the petri dish, $RSP2_{1-120}$ strains and the control accumulated at equal rates toward light of ambient intensity to 4 klx, a typical positive phototaxis. The cells accumulated away from light of higher intensity (20 klx) as negative phototaxis. The opposite responses to different light intensities were reversible. In addition, all displayed similar phototaxis to a narrow light beam parallel to the glass surface, a method of assaying phototaxis under a microscope (38). Furthermore, all exhibited photoshock in response to a flash of strong white light (22, 38). We reasoned that the irregular trajectory of $RSP2_{1-120}$ cells might be a different response in which light drove them toward the perpendicularly oriented glass surface under regular microscopes. If this prediction was correct, the irregularity of the trajectory would be less if light was parallel to the glass surface. To test this, we altered the light direction by using a gooseneck lamp that was also equipped with a tungsten light bulb, like our light microscopes (Fig. 8B, schematic). Although this light beam without a condenser was less focused than the microscope light source, the irregular trajectory was not striking under the horizontal illumination even at 6 klx (top). However, when the illumination was turned to a vertical orientation (bottom), $RSP2_{1-120}$ cells immediately moved irregularly, presumably a heightened response of the light-driven $RSP2_{1-120}$ cells when they encountered glass. Under this condition, the trajectories of control cells also appeared more irregular, but the irregularity was less pronounced than in the $RSP2_{1-120}$ cells (Fig. 8B, compare the two right images).

Abnormal orientation and asynchronous flagella of $RSP2_{1-120}$ cells. To elucidate the cause of this new light-dependent phenotype, we carried out high-speed video microscopy with bright illumination (>20 klx) perpendicular to the glass surface (Fig. 9A; see Videos 4 and 5 in the supplemental material). Like wild-type strains (51, 66), under such conditions, the control swimmers moved in a helical trajectory with an oval cell body and synchronized flagella with an asymmetrical waveform (Fig. 9A, top). We also noticed that the swimmers were in different focal planes. In contrast, $RSP2_{1-120}$ swimmers were largely concentrated near the glass slide (bottom). Their flagella beat asynchronously, even though they were not stuck, while their cell bodies appeared spherical unless they were turning. This suggested that the control cells and $RSP2_{1-120}$ cells were oriented differently under the microscope.

The montage of time-lapse images, 1 per 20 frames (about one of every two beat cycles), showed the progressive movement along a curved path of a typical control cell with an oval cell body (Fig. 9B, top). The synchronized flagella and pyrenoid (white arrow) were at opposite ends of the oval cell body. In contrast, $RSP2_{1-120}$ cells with unsynchronized flagella did not translocate much horizontally (Fig. 9B, bottom). The proximal ends of the flagella were obscured, while the pyrenoid appeared near the center of a spher-

TABLE 2 Light-induced irregular movement of $RSP2_{1-120}$ cells is calcium dependent[a]

	Trajectory in:					
	Growth medium		HEPES (10 mM), EGTA (0.4 mM)		HEPES (10 mM), calcium (1 mM)	
Strain	D	N	D	N	D	N
WT	HS	HS	HS	HS	HS	HS
Cont	HS	HS	HS	HS	HS	HS
1-120	HS	IS	HS	HS	HS	IS

[a] WT, Cont, and $RSP2_{1-120}$ cells from log-phase cultures were resuspended in growth medium or HEPES with or without EGTA and calcium. The swimming behaviors of these cells were recorded under dim (D; ~0.1 klx) and normal (N; ~1 klx) light intensities. WT and Cont cells swam helically in the presence and absence of calcium, while $RSP2_{1-120}$ cells displayed irregular motility only in the presence of calcium. HS, helical swimming; IS, irregular swimming.

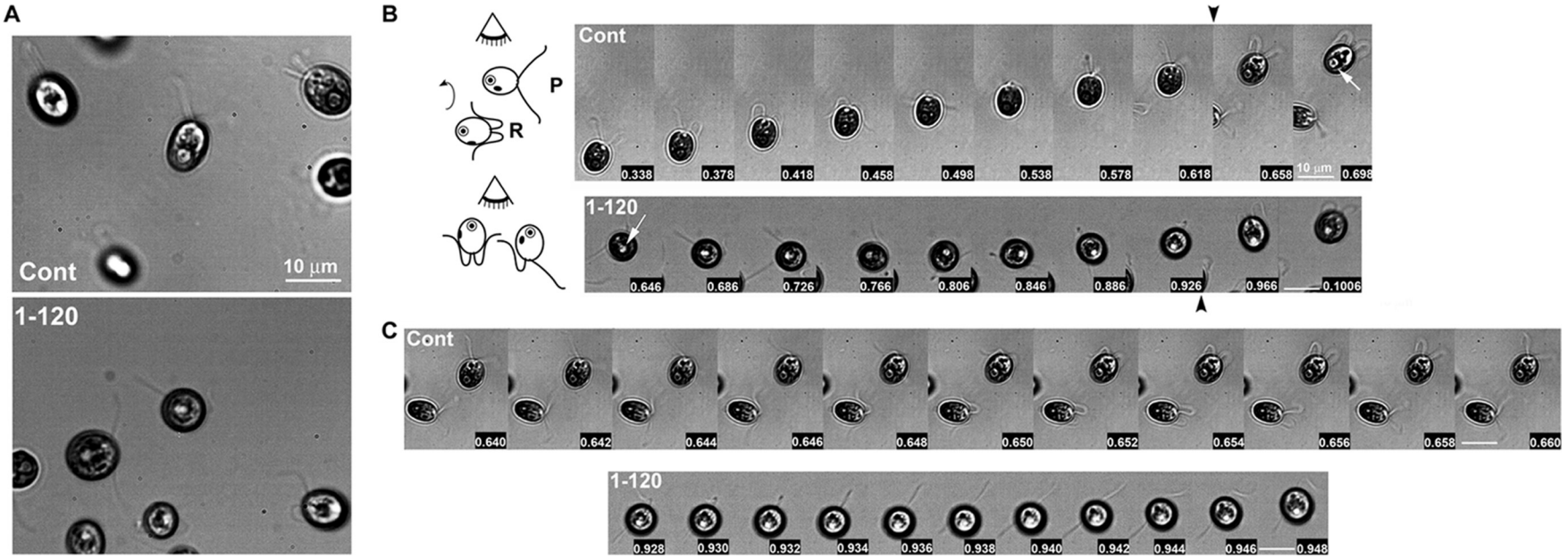

FIG 9 Distinct orientations and flagellar asynchrony of $RSP2_{1\text{-}120}$ cells and control cells when the illumination was perpendicular to the glass surface. (A) A representative image from high-speed video microscopy of wild-type control cells (Cont) and $RSP2_{1\text{-}120}$ cells (1-120). Control cells, mostly appearing oval, were at different focal planes, and their flagella beat synchronously with a breast stroke-like waveform. $RSP2_{1\text{-}120}$ cells mostly appeared spherical in a similar focal plane near the slide. The two flagella of most $RSP2_{1\text{-}120}$ cells beat asynchronously. The image was captured at a rate of ~500 frames/s. (B) Time-lapse footage compiled from 1 per 20-frame images of a single cell and the corresponding schematic (left). A typical oval control cell (top) with flagella beating synchronously, with alternate power (P) and recovery (R) strokes, progressed in a helical path while simultaneously rotating (curved arrow) along the cell body axis. The pyrenoid granule (white arrow) and flagella were at opposite ends of the cell. The flagella of an $RSP2_{1\text{-}120}$ cell (bottom) were initially unsynchronized and partially hidden by the spherical cell body with a pyrenoid in the center. The $RSP2_{1\text{-}120}$ cell translocated modestly until it was turning, as shown in the last few images. The turning cells appeared oval, with two flagella beating synchronously. The consecutive images taken between two frames (arrowheads) are shown in panel C. (C) A beat cycle of two control cells with synchronous flagella (top) and an $RSP2_{1\text{-}120}$ cell with asynchronous flagella (bottom). The time is stamped in seconds. These footages indicate that control cells tend to position and swim parallel to the glass slide; $RSP2_{1\text{-}120}$ cells tended to be oriented perpendicular to the glass surface and faced the light directly (schematics), with unsynchronized flagella that were partly obscured by the cell body.

ical cell body. Near the end of the footage, this $RSP2_{1-120}$ cell with synchronized flagella was pulling into a horizontal position. These images suggest that control cells tend to swim horizontally, with the cell body axis parallel to the glass, whereas $RSP2_{1-120}$ cells switch between this horizontal direction (oval) and the vertical orientation (spherical, toward light) (schematics in Fig. 9B). The consecutive images between the two frames (indicated by arrowheads) demonstrate the movement of two synchronous flagella in a complete beat cycle of the control cell (Fig. 9C, top) and the asynchronous beat of a turning $RSP2_{1-120}$ cell (Fig. 9C, bottom). Recordings of cells from stationary-phase cultures that were less light sensitive showed that the waveforms and beat frequencies of $RSP2_{1-120}$ cells and control cells were similar. These observations strongly suggest that $RSP2_{1-120}$ cells tend to be oriented perpendicular to the glass surface but repeatedly attempt to swim away from the confronting glass and light, leading to the irregular trajectory. In contrast, under the same conditions, the control cells could swim a long distance horizontally between the glass surfaces, not being brought to the glass surface repeatedly by phototaxis.

DISCUSSION

RSP2's DPY-30 domain targets a helix for the assembly of the spokehead region. This study demonstrates three functional units in RSP2: the DPY-30 domain, the adjacent helix, and the C-terminal extension (Fig. 3). $RSP2_{1-120}$, with only the first two modules, restores missing RSPs to pf24 flagella (Fig. 6) and rescues motility (Fig. 8), indicating that this short fragment is sufficient for RS assembly and normal oscillatory beating. This finding suggests that DYDC2, which is similar to this region and is found in the cilium proteome (Fig. 3C), is an RSP2 orthologue and that its gene is a candidate gene for primary cilium dyskinesia, a congenital syndrome due to dysmotile cilia (19). Importantly, the function of this region is not limited to the DPY-30 domain, since the RS composition is also restored in the paralyzed flagella lacking the domain (ΔDPY) (Fig. 6). Therefore, the DPY-30 domain's adjacent helix in both RSP2 and DYDC2 is involved in RS assembly, possibly forming a coiled coil with an unknown spoke protein. However, without the DPY-30 domain, the assembly is faulty, as flagella are still paralyzed (Fig. 5) and the restored ΔDPY polypeptide and the other RSPs dissociate in 0.6 M KI buffer (66) (Fig. 7). The tight association of DPY-30 domain-containing $RSP2_{1-120}$ and RSP23 with the stalk (Fig. 7) strongly suggests that DPY-30 domains, like RIIa domains, mediate docking, as well. In the case of RSP2, it docks the flanking helix and the associated proteins to the stalk for RS assembly. We cannot exclude the possibility that there is some form of interallelic complementation between mutated RSP2 polypeptides expressed by transgenes and the trace amounts of the full-length RSP2 endogenous to the parental strain. However, given their disparate stoichiometry and their structural roles, we favor the hypothesis that $RSP2_{1-120}$, with the first two functional units, is sufficient for RS assembly and that the calmodulin-binding region has a primary role in the regulation of swimming.

We propose a working model to explain this assembly role. The DPY-30 domain dimer (twin gray circles in Fig. 10A, left) and the adjacent short helices (two gray rectangles) function as a two-prong structural linker for the head-stalk connection in the RS. The D/D domain binds to a site in one chain of an unknown dimeric RSP (black and gray lines), possibly analogous to the interaction between RIIa and AKAPs (4). The same site in the other chain may anchor the DPY-30 domain in NDK-5 (RSP23). The docking ensures proper coiled-coil formation between the helices in the RSP2 dimer and in its dimeric anchors. The four helices further associate with the two spokehead paralogues, RSP4 and RSP6 (large open circles in the middle), which are deficient in ΔCT-Tag axonemes (Fig. 6). This model provides the molecular explanation for a symmetrical Y-shaped spokehead-neck area in traditional and cryoelectron micrographs (Fig. 1) (3, 24, 46) and multiple short helices in the splayed spokehead (50). Additionally, it explains chemical cross-linking of RSP2 and spokehead proteins (32) and at least two proteins involved in the head-stalk connection (70). This subcomplex could further associate with other spoke proteins, such as the dimeric spoke HSP40, which depends on RSP2 for assembly (27). Notably, both HSP40 and the DPY-30 domain are dispensable for normal RS composition (66, 70), yet flagella that lack either one jerk and cross each other sporadically (Fig. 5), suggesting disrupted sequential activation of axonemal dyneins (66). We envision that without either dimeric element, the multiple molecules near the spokehead, though assembled, cannot fold into the sturdy unit (Fig. 10A, right) required for timely intermittent coupling between the CP and motors at the outer doublets during rhythmic beating, leading to sporadic stalling of jerky flagella.

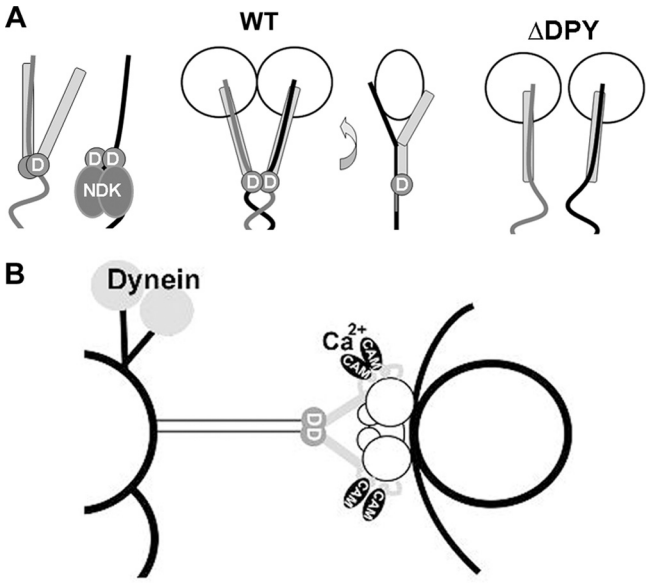

FIG 10 Models depicting the roles of the molecular moieties in RSP2. (A) A two-prong structural linker model of $RSP2_{1-120}$. (Left) One chain of an unknown dimeric protein (lines) anchors the dimeric DPY-30 domain (gray circles labeled D) that tethers the flanking helices (gray rectangles). The other chain of the anchoring protein anchors the DPY-30 domains in dimeric NDK-5. (Middle) Docking of DPY-30 facilitates the flanking sequences in dimeric RSP2 and the dimeric anchoring protein forming coiled coils, thus forming a dimeric platform for a symmetric complex. The four polypeptides then recruit two spokehead paralogues (open circles; see the 90° view). The DPY-30-containing NDK5 is not illustrated for clarity. (Right) Without the DPY-30 domain, the dimeric platform is uncoupled and unstable. (B) Effects of calcium on RSP2's C-terminal tail and the radial spoke. The tail interacts with both calmodulin (CAM) and the spokehead. Calcium alters these interactions, modulating the intermittent contact between RS and the central pair. Only part of the 9 + 2 axoneme is illustrated.

The dispensable calmodulin-binding region enhances spokehead stability and steering. Although RSP2's C-terminal extension is absent in most RSP2-like molecules and is not needed for oscillatory beating, it may serve an intriguing function for *Chlamydomonas*—steering under perpendicular bright illumination and glass surfaces. While control swimmers can maintain helical trajectories parallel to the glass surface, seemingly momentarily unresponsive to incident light, $RSP2_{1\text{-}120}$ cells lacking this region cluster near the glass slide, turning repeatedly with asynchronous flagella (Fig. 8 and 9). This phenotype is unusual in several respects. $RSP2_{1\text{-}120}$ strains are the first RS or CP mutants that are fully motile. Despite the steering anomaly, their velocities (Table 1) and the frequencies and waveforms of their flagella are within normal ranges (Fig. 9). In contrast, dynein mutants that swim with distinct trajectories have lower beat frequencies, shallower bend amplitudes, and lower velocities (55). This phenotype provides the evidence that fine-tuning the RS/CP control system could affect synchrony and trajectories with a mechanism independent of the waveform or beat frequency.

As flagellum-propelled movements are mercurial and remain poorly understood (29, 47), we tentatively offer several speculations regarding the asynchrony and steering anomaly of $RSP2_{1\text{-}120}$ cells. This reminded us of the spinning tendency of a transgenic mutant defective in a calcium-binding motif of an outer dynein docking protein (9). While these two strains exhibit intriguing behaviors under light microscopes, both appear normal in all other respects, including phototaxis and photoshock (25). Although these two light-induced responses are the best-characterized calcium-induced motility changes (55), there are clearly more calcium-induced flagellar behaviors (5, 7, 56, 58). Perhaps the more than 30 calcium- and calmodulin-binding axonemal proteins (35, 45) enable axonemes to generate an array of calcium-induced changes under various circumstances, some as a single switch while the others act in concert. As such, the mutation of a potential calcium sensor may not exactly abolish phototaxis or photoshock.

The steering anomaly of $RSP2_{1\text{-}120}$ cells is correlated with the reduced stability of their spoke heads (Fig. 7). RSP2's C-terminal extension may locally affect the spokehead to influence steering. The spokehead contacts the CP intermittently, and the contact is crucial for flagellar beating and synchrony (62, 66). It has been shown that bright light selectively enhances the inherent asynchrony of only one (*trans*) flagellum of an algal cell (29, 47). Perhaps RSP2's C-terminal tail and calmodulin strengthen the spokehead, constitutively or in a calcium-dependent manner, to regulate the asynchrony rate. The inherent asynchronous incidence in $RSP2_{1\text{-}120}$ cells may be slightly different from that of the control, and the asynchronous tendency simply worsens or is sufficient to prevent them from turning properly under the conflicting stimuli of strong light and sticky barriers. Another interesting possibility is that this region is part of a swim-to-glide switching mechanism that is calcium dependent and that involves the RS and the CP. When wild-type cells are stuck to the glass, the flagella first become quiescent and then glide along the glass surface (5, 36). Perhaps for control cells that manage to swim away the increased intraflagellar calcium from encountering glass alters RSP2/calmodulin interactions and thus modulates the RS/CP control system (Fig. 10B), momentarily blocking phototactic turns and enabling the escapees to swim across the optic field. In contrast, $RSP2_{1\text{-}120}$ cells may be less likely to become quiescent and more likely to remain free swimming and phototactic, thus repeatedly turning to light and reencountering the glass. Regardless of the precise mechanisms, the *Chlamydomonas*-unique tail in RSP2 could be considered one of the emerging mechanisms by which a cell responds to simultaneous stimuli (12). We are currently devising strategies to test these possibilities.

In conclusion, RSP2 is comprised of multiple modules, like calmodulin-binding proteins in the actin cytoskeletal system (59). In the case of RSP2, the D/D domain docks a helix for RS assembly, and its special calmodulin-binding tail modulates the spokehead, enabling the biflagellate green alga to steer in a unique situation. These roles in shaping and changing RS structure are a conceptual departure from docking PKA and provide another example showing that domain recombination drives the evolution of organismal complexity (11): certain domains tend to associate with each other, and the mix-and-match scheme reduces the need to evolve entirely novel molecules. However, the rationales for docking various functional moieties via D/D domains may be identical. While docking PKA enhances the spatial and temporal precision of its promiscuous enzymatic activity, we speculate that docking structural modules, especially helices with coiled-coil propensity, enhances accuracy and efficiency in molecular interactions. In addition, the dimeric domain may be one of the tools to form a symmetric complex, like the RS head (Fig. 1 and 10). These structural roles and the versatility of D/D domains explain the fact that cilia and flagella are enriched with RIIa clan members (8, 21, 40). They may be used to form symmetric complexes in the cytoskeletons of these organelles. Furthermore, the diverged sequences provide a means to evolve cell-type-specific motility via the seemingly identical 9 + 2 axoneme (46, 49, 55). It remains to be seen if the structural role is also applicable to the small dimeric DPY-30 protein (60) that specifically affects H3K4 trimethylation (28) but lacks any other noticeable feature.

ACKNOWLEDGMENTS

We thank Kathleen Karrer (Marquette University) for critical comments on the manuscript, Carolyn D. Silflow (University of Minnesota) for providing the p3HA plasmid, Stephen M. King (University of Connecticut Health Center) for providing the anti-RSP23 antibody, and Mark I. Donnelly (Argonne National Laboratory) for providing MBP-tagged truncated RSP2 constructs.

This work was supported by NIH grants GM068101, GM068101-05A1, and GM090162 (to P.Y.) and NSF PHY-0848763 (to K.W.F.).

REFERENCES

1. **Aravind L, Ponting CP.** 1997. The GAF domain: an evolutionary link between diverse phototransducing proteins. Trends Biochem. Sci. **22**: 458–459.
2. **Arnaiz O, et al.** 2009. Cildb: a knowledgebase for centrosomes and cilia. Database (Oxford) **2009**:bap022. doi:10.1093/database/bap022.
3. **Barber CF, Heuser T, Carbajal-Gonzalez BI, Botchkarev VV, Jr, Nicastro D.** 2012. Three-dimensional structure of the radial spokes reveals heterogeneity and interactions with dyneins in Chlamydomonas flagella. Mol. Biol. Cell **23**:111–120.
4. **Beene DL, Scott JD.** 2007. A-kinase anchoring proteins take shape. Curr. Opin. Cell Biol. **19**:192–198.
5. **Bloodgood RA, Salomonsky NL.** 1990. Calcium influx regulates antibody-induced glycoprotein movements within the Chlamydomonas flagellar membrane. J. Cell Sci. **96**:27–33.
6. **Brokaw CJ, Luck DJ, Huang B.** 1982. Analysis of the movement of Chlamydomonas flagella: the function of the radial-spoke system is revealed by comparison of wild-type and mutant flagella. J. Cell Biol. **92**: 722–732.

7. **Brokaw CJ, Nagayama SM.** 1985. Modulation of the asymmetry of sea urchin sperm flagellar bending by calmodulin. J. Cell Biol. **100**:1875–1883.
8. **Carr DW, et al.** 2001. Identification of sperm-specific proteins that interact with A-kinase anchoring proteins in a manner similar to the type II regulatory subunit of PKA. J. Biol. Chem. **276**:17332–17338.
9. **Casey DM, Yagi T, Kamiya R, Witman GB.** 2003. DC3, the smallest subunit of the Chlamydomonas flagellar outer dynein arm-docking complex, is a redox-sensitive calcium-binding protein. J. Biol. Chem. **278**:42652–42659.
10. **Cho YW, et al.** 2007. PTIP associates with MLL3- and MLL4-containing histone H3 lysine 4 methyltransferase complex. J. Biol. Chem. **282**:20395–20406.
11. **Chothia C, Gough J, Vogel C, Teichmann SA.** 2003. Evolution of the protein repertoire. Science **300**:1701–1703.
12. **Coba MP, et al.** 2009. Neurotransmitters drive combinatorial multistate postsynaptic density networks. Sci. Signal. **2**:ra19.
13. **Curry AM, Williams BD, Rosenbaum JL.** 1992. Sequence analysis reveals homology between two proteins of the flagellar radial spoke. Mol. Cell. Biol. **12**:3967–3977.
14. **Diener DR, Ang LH, Rosenbaum JL.** 1993. Assembly of flagellar radial spoke proteins in Chlamydomonas: identification of the axoneme binding domain of radial spoke protein 3. J. Cell Biol. **123**:183–190.
15. **Diener DR, et al.** 2011. Sequential assembly of flagellar radial spokes. Cytoskeleton **68**:389–400.
16. **DiPetrillo CG, Smith EF.** 2010. Pcdp1 is a central apparatus protein that binds Ca(2+)-calmodulin and regulates ciliary motility. J. Cell Biol. **189**:601–612.
17. **Donnelly MI, et al.** 2006. An expression vector tailored for large-scale, high-throughput purification of recombinant proteins. Protein Expr. Purif. **47**:446–454.
18. **Dymek EE, Smith EF.** 2007. A conserved CaM- and radial spoke-associated complex mediates regulation of flagellar dynein activity. J. Cell Biol. **179**:515–526.
19. **Fliegauf M, Benzing T, Omran H.** 2007. When cilia go bad: cilia defects and ciliopathies. Nat. Rev. Mol. Cell Biol. **8**:880–893.
20. **Foster KW.** 2009. Analysis of the ciliary/flagellar beating of *Chlamydomonas*. Methods Cell Biol. **91**:173–239.
21. **Fujita A, et al.** 2000. Ropporin, a sperm-specific binding protein of rhophilin, that is localized in the fibrous sheath of sperm flagella. J. Cell Sci. **113**:103–112.
22. **Fujiu K, Nakayama Y, Yanagisawa A, Sokabe M, Yoshimura K.** 2009. Chlamydomonas CAV2 encodes a voltage-dependent calcium channel required for the flagellar waveform conversion. Curr. Biol. **19**:133–139.
23. **Gold MG, et al.** 2006. Molecular basis of AKAP specificity for PKA regulatory subunits. Mol. Cell **24**:383–395.
24. **Goodenough UW, Heuser JE.** 1985. Substructure of inner dynein arms, radial spokes, and the central pair/projection complex of cilia and flagella. J. Cell Biol. **100**:2008–2018.
25. **Hegemann P, Berthold P.** 2009. Sensory photoreceptors and light control of flagellar activity, p 396–429. *In* Witman GB (ed), *Chlamydomonas* sourcebook, 2nd ed, vol 3. Elsevier Inc., Oxford, United Kingdom.
26. **Hsu DR, Chuang PT, Meyer BJ.** 1995. DPY-30, a nuclear protein essential early in embryogenesis for Caenorhabditis elegans dosage compensation. Development **121**:3323–3334.
27. **Huang B, Piperno G, Ramanis Z, Luck DJ.** 1981. Radial spokes of Chlamydomonas flagella: genetic analysis of assembly and function. J. Cell Biol. **88**:80–88.
28. **Jiang H, et al.** 2011. Role for Dpy-30 in ES cell-fate specification by regulation of H3K4 methylation within bivalent domains. Cell **144**:513–525.
29. **Josef K, Saranak J, Foster KW.** 2005. An electro-optic monitor of the behavior of Chlamydomonas reinhardtii cilia. Cell Motil. Cytoskeleton **61**:83–96.
30. **Kammerer S, et al.** 2003. Amino acid variant in the kinase binding domain of dual-specific A kinase-anchoring protein 2: a disease susceptibility polymorphism. Proc. Natl. Acad. Sci. U. S. A. **100**:4066–4071.
31. **King SJ, Dutcher SK.** 1997. Phosphoregulation of an inner dynein arm complex in Chlamydomonas reinhardtii is altered in phototactic mutant strains. J. Cell Biol. **136**:177–191.
32. **Kohno T, Wakabayashi K, Diener DR, Rosenbaum JL, Kamiya R.** 2011. Subunit interactions within the Chlamydomonas flagellar spokehead. Cytoskeleton **68**:237–246.
33. **Lecroisey A, Lascu I, Bominaar A, Veron M, Delepierre M.** 1995. Phosphorylation mechanism of nucleoside diphosphate kinase: 31P-nuclear magnetic resonance studies. Biochemistry **34**:12445–12450.
34. **Lieb JD, Capowski EE, Meneely P, Meyer BJ.** 1996. DPY-26, a link between dosage compensation and meiotic chromosome segregation in the nematode. Science **274**:1732–1736.
35. **Merchant SS, et al.** 2007. The Chlamydomonas genome reveals the evolution of key animal and plant functions. Science **318**:245–250.
36. **Mitchell BF, Grulich LE, Mader MM.** 2004. Flagellar quiescence in Chlamydomonas: characterization and defective quiescence in cells carrying sup-pf-1 and sup-pf-2 outer dynein arm mutations. Cell Motil. Cytoskeleton **57**:186–196.
37. **Mitchell DR, Rosenbaum JL.** 1985. A motile Chlamydomonas flagellar mutant that lacks outer dynein arms. J. Cell Biol. **100**:1228–1234.
38. **Moss AG, Pazour GJ, Witman GB.** 1995. Assay of Chlamydomonas phototaxis. Methods Cell Biol. **47**:281–287.
39. **Nagy PL, Griesenbeck J, Kornberg RD, Cleary ML.** 2002. A trithorax-group complex purified from Saccharomyces cerevisiae is required for methylation of histone H3. Proc. Natl. Acad. Sci. U. S. A. **99**:90–94.
40. **Newell AE, et al.** 2008. Protein kinase A RII-like (R2D2) proteins exhibit differential localization and AKAP interaction. Cell Motil. Cytoskeleton **65**:539–552.
41. **Okita N, Isogai N, Hirono M, Kamiya R, Yoshimura K.** 2005. Phototactic activity in Chlamydomonas 'non-phototactic' mutants deficient in Ca2+-dependent control of flagellar dominance or in inner-arm dynein. J. Cell Sci. **118**:529–537.
42. **Ostrowski LE, et al.** 2002. A proteomic analysis of human cilia: identification of novel components. Mol. Cell. Proteomics **1**:451–465.
43. **Otter, T.**1989. Calmodulin and the control of flagellar movement, p 281–298. *In* Warner FD, Satir P, Gibbons IR (ed), Cell movement, vol 1. Alan R. Liss, New York, NY.
44. **Patel-King RS, Gorbatyuk O, Takebe S, King SM.** 2004. Flagellar radial spokes contain a Ca2+-stimulated nucleoside diphosphate kinase. Mol. Biol. Cell **15**:3891–3902.
45. **Pazour GJ, Agrin N, Leszyk J, Witman GB.** 2005. Proteomic analysis of a eukaryotic cilium. J. Cell Biol. **170**:103–113.
46. **Pigino G, et al.** 2011. Cryoelectron tomography of radial spokes in cilia and flagella. J. Cell Biol. **195**:673–687.
47. **Polin M, Tuval I, Drescher K, Gollub JP, Goldstein RE.** 2009. Chlamydomonas swims with two "gears" in a eukaryotic version of run-and-tumble locomotion. Science **325**:487–490.
48. **Porter ME, Sale WS.** 2000. The 9 + 2 axoneme anchors multiple inner arm dyneins and a network of kinases and phosphatases that control motility. J. Cell Biol. **151**:F37–F42.
49. **Publicover S, Harper CV, Barratt C.** 2007. [Ca2+]i signalling in sperm—making the most of what you've got. Nat. Cell Biol. **9**:235–242.
50. **Qin H, Diener DR, Geimer S, Cole DG, Rosenbaum JL.** 2004. Intraflagellar transport (IFT) cargo: IFT transports flagellar precursors to the tip and turnover products to the cell body. J. Cell Biol. **164**:255–266.
51. **Rüffer U, Nultsch W.** 1985. High-speed cinematographic analysis of the movement of Chlamydomonas. Cell Motil. Cytoskeleton **5**:251–263.
52. **Segal RA, Luck DJ.** 1985. Phosphorylation in isolated Chlamydomonas axonemes: a phosphoprotein may mediate the Ca2+-dependent photophobic response. J. Cell Biol. **101**:1702–1712.
53. **Shimogawara K, Fujiwara S, Grossman A, Usuda H.** 1998. High-efficiency transformation of Chlamydomonas reinhardtii by electroporation. Genetics **148**:1821–1828.
54. **Silflow CD, et al.** 2001. The Vfl1 protein in Chlamydomonas localizes in a rotationally asymmetric pattern at the distal ends of the basal bodies. J. Cell Biol. **153**:63–74.
55. **Smith EF, Yang P.** 2004. The radial spokes and central apparatus: mechano-chemical transducers that regulate flagellar motility. Cell Motil. Cytoskeleton **57**:8–17.
56. **Smyth RD, Berg HC.** 1982. Change in flagellar beat frequency of Chlamydomonas in response to light. Prog. Clin. Biol. Res. **80**:211–215.
57. **Stolc V, Samanta MP, Tongprasit W, Marshall WF.** 2005. Genome-wide transcriptional analysis of flagellar regeneration in Chlamydomonas reinhardtii identifies orthologs of ciliary disease genes. Proc. Natl. Acad. Sci. U. S. A. **102**:3703–3707.
58. **Wakabayashi KI, Ide T, Kamiya R.** 2009. Calcium-dependent flagellar motility activation in Chlamydomonas reinhardtii in response to mechanical agitation. Cell Motil. Cytoskeleton **66**:736–742.

59. **Wang CL.** 2008. Caldesmon and the regulation of cytoskeletal functions. Adv. Exp. Med. Biol. **644**:250–272.
60. **Wang X, et al.** 2009. Crystal structure of the C-terminal domain of human DPY-30-like protein: a component of the histone methyltransferase complex. J. Mol. Biol. **390**:530–537.
61. **Wargo MJ, Dymek EE, Smith EF.** 2005. Calmodulin and PF6 are components of a complex that localizes to the C1 microtubule of the flagellar central apparatus. J. Cell Sci. **118**:4655–4665.
62. **Warner FD, Satir P.** 1974. The structural basis of ciliary bend formation. Radial spoke positional changes accompanying microtubule sliding. J. Cell Biol. **63**:35–63.
63. **Wei M, Sivadas P, Owen HA, Mitchell DR, Yang P.** 2010. Chlamydomonas mutants display reversible deficiencies in flagellar beating and axonemal assembly. Cytoskeleton **67**:71–80.
64. **Wu N, et al.** 2006. Soluble mimics of the cytoplasmic face of the human V1-vascular vasopressin receptor bind arrestin2 and calmodulin. Mol. Pharmacol. **70**:249–258.
65. **Xu Z, et al.** 2009. A role of histone H3 lysine 4 methyltransferase components in endosomal trafficking. J. Cell Biol. **186**:343–353.
66. **Yang C, Owen HA, Yang P.** 2008. Dimeric heat shock protein 40 binds radial spokes for generating coupled power strokes and recovery strokes of 9 + 2 flagella. J. Cell Biol. **180**:403–415.
67. **Yang C, Yang P.** 2006. The flagellar motility of Chlamydomonas pf25 mutant lacking an AKAP-binding protein is overtly sensitive to medium conditions. Mol. Biol. Cell **17**:227–238.
68. **Yang P, Diener DR, Rosenbaum JL, Sale WS.** 2001. Localization of calmodulin and dynein light chain LC8 in flagellar radial spokes. J. Cell Biol. **153**:1315–1326.
69. **Yang P, et al.** 2006. Radial spoke proteins of Chlamydomonas flagella. J. Cell Sci. **119**:1165–1174.
70. **Yang P, Yang C, Sale WS.** 2004. Flagellar radial spoke protein 2 is a calmodulin binding protein required for motility in Chlamydomonas reinhardtii. Eukaryot. Cell **3**:72–81.
71. **Yap KL, et al.** 2000. Calmodulin target database. J. Struct. Funct. Genomics **1**:8–14.
72. **Yokoyama R, O'Toole E, Ghosh S, Mitchell DR.** 2004. Regulation of flagellar dynein activity by a central pair kinesin. Proc. Natl. Acad. Sci. U. S. A. **101**:17398–17403.